In Situ X-ray Diffraction and Solid-State NMR Study of the Fluorination of γ-Al_2O_3 with HCF_2Cl

Peter J. Chupas, Michael F. Ciraolo, Jonathan C. Hanson,† and Clare P. Grey*

Contribution from the Department of Chemistry, State University of New York at Stony Brook, Stony Brook, New York 11794-3400

Received August 31, 2000

Abstract: In situ X-ray diffraction (XRD) and NMR methods were used to follow the structural changes that occur during the dismutation reaction of hydrochlorofluorocarbon-22 ($CHClF_2$) over γ-alumina. Use of a flow cell allowed diffraction patterns to be recorded, while the reaction products were simultaneously monitored downstream of the catalyst bed, by gas chromatography. No visible structural changes of γ-Al_2O_3 were observed at 300 °C, the temperature at which this material becomes active for catalysis. A new phase began to form at 360 °C, which by 500 °C completely dominated the XRD powder pattern. $^{19}F/^{27}Al$ cross-polarization (CP) experiments of γ-Al_2O_3 activated at 300 °C showed that AlF_3 had already begun to form at this temperature. By 400 °C, resonances from a phase that resembles α-AlF_3 dominate both the ^{19}F and ^{27}Al NMR spectra of the used catalyst. In situ XRD experiments of the catalytically inactive α-AlF_3 phase were performed to investigate the structural changes of this material, associated with the extent of tilting of the AlF_6 octahedra in this ReO_3-related structure, as a function of temperature. Structural refinements of this sample, and the catalytically active phase that grows over γ-Al_2O_3, demonstrate that the catalyst is structurally similar to the rhombohedral form of α-AlF_3. Differences between the two phases are ascribed to defects in the catalyst, which limit the flexibility of the structure; these may also be responsible for the differences in the catalytic behavior of the two materials.

Introduction

The need to develop environmentally friendly alternatives to chlorofluorocarbons (CFC) has resulted in the discovery of new catalyzed halogen-exchange, elimination, and isomerization reactions.[1] Many of the catalytic reactions that occur over metal oxides require activation periods that can involve considerable structural and chemical changes and, depending on the gas used for activation (usually a halocarbon), O/F or O/Cl exchange on the surface. For example, one method used for the production of catalytically active materials involves the fluorination of aluminas with fluorinating agents such as HF or fluorocarbons.[2−4] Trifluoromethane (HFC-23) has been used in the fluorination of γ-Al_2O_3 at 400 and 500 °C, to obtain a material that resembles α-AlF_3.[4,5] CFCs or HCFCs may similarly be used to fluorinate metal oxides, but these gases also serve as a measure of the material's subsequent catalytic activity. For example, the dismutation (i.e., disproportionation) reaction of HCFC-22 ($CClF_2H$) ($3CClF_2H \rightarrow 2CF_3H + CCl_3H$) over both chromium and aluminum catalysts has been widely used as a model reaction with which to investigate the mechanisms of fluorination and catalysis.[2] This reaction was, therefore, investigated over a γ-Al_2O_3 catalyst in the work reported in this paper.

IR spectroscopy studies of chemisorbed CFC molecules on alumina surfaces have revealed that the molecules chemisorb following C−Cl bond breakage. This is consistent with the following bond dissociation energies, C−H (439 kJ mol^{-1}), C−Cl (354 kJ mol^{-1}), and C−F (460 kJ mol^{-1}),[6] which clearly demonstrate that the C−Cl bond is the weakest bond in a CFC or HCFC molecule. Thus, the addition of a C−Cl bond to the fluorinating gas enables both fluorination of the surface and reactivity at lower temperatures, leading to the destruction of the CFC molecule and the production of CO_2.[7] Based on the previous study of CFC-114a,[7] breaking of the C−Cl bond in HCFC-22 should result in formation of a surface bound $-O-CF_2H$ species, followed by subsequent fluorination of the surface.

The thermodynamically stable aluminum fluoride phase, α-AlF_3, adopts a rhombohedral structure ($R\bar{3}c$, Figure 1a) at room temperature, and is reported to undergo a first-order phase transition at approximately 460 °C to the cubic α-ReO_3 structure (Pm-3m, Figure 1b).[8,9] In the high-temperature cubic phase, all the AlF_6 octahedra are connected via bridging (corner shared) fluorine atoms with Al−F−Al bond angles of 180 °, while the octahedra are tilted along their 3-fold axis in the low-temperature rhombohedral phase, resulting in zigzag chains of octahedra and Al−F−Al bond angles of 157.9 °. Many metastable phases of AlF_3 have also been reported, their synthesis involving the

† Chemistry Department, Brookhaven National Laboratory, Upton, NY 11973.

(1) Manzer, L. E. *Science* **1990**, *249*, 31−35. Manzer, L. E.; Rao, V. N. M. Catalytic Synthesis of CFC Alternatives. *Adv. Catal.* **1993**, *39*, 329.
(2) Kemnitz, E.; Menz, D. H. *Prog. Solid State Chem.* **1998**, *26*, 97−153.
(3) Hess, A.; Kemnitz, E. *J. Catal.* **1994**, *149*, 449−457.
(4) McVicker, G. B.; Kim, C. J.; Eggert, J. J. *J. Catal.* **1983**, *80*, 315−327.
(5) Hegde, R. I.; Barteau, M. A. *J. Catal.* **1989**, *120*, 387−400.
(6) McMillan, D. F.; Golden, D. M. *Annu. Rev. Phys. Chem.* **1982**, 33, 493−532.
(7) Deshmukh, S. S.; Kovalchuk, V. I.; Borovkov, V. Y.; d'Itri, J. L. *J. Phys. Chem. B* **2000**, *104*, 1277−1284.
(8) Daniel, P.; Bulou, A.; Rousseau, M.; Nouet, J.; Fourquet, J. L.; Leblanc, M.; Burriel, R. *J. Phys.: Condens. Matter* **1990**, *2*, 5663−5677.
(9) Ravez, J.; Mogus-Milankovic, A.; Chaminade, J. P.; Hagenmuller, P. *Mater. Res. Bull.* **1984**, *19*, 1311−1316.

10.1021/ja0032374 CCC: $20.00
Published on Web 02/02/2001

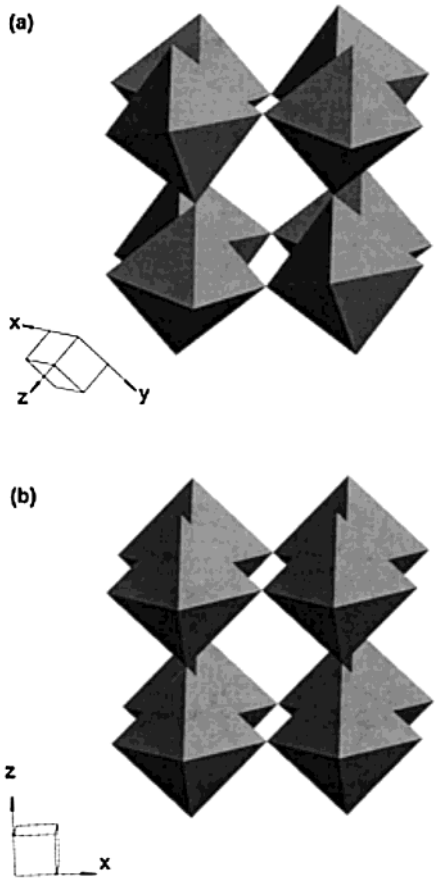

Figure 1. (a) Room temperature structure of α-AlF_3 and the (b) cubic α-AlF_3 structure.

decomposition of hydrated AlF_3 species or the use of soft chemistry. β-AlF_3 can be synthesized through the decomposition of α-$AlF_3 \cdot 3H_2O$ or α-NH_4AlF_3, and is isostructural with other β-MF_3 (M = Fe, Cr, Ir, Ge) compounds which all adopt a slightly distorted, hexagonal tungsten-bronze structures.[2,10] The reported decomposition of $N(CH_3)_4AlF_4 \cdot H_2O$ leads to t-AlF_3, which is identical to θ-AlF_3 (produced through the decomposition of $N(CH_3)_4AlF_4$).[11,12] Additionally, the use of soft chemistry methods has led to the synthesis of the κ and η phases.[12] A multitude of other less well-substantiated phases have also been reported (γ(2), δ, ϵ), which most likely represent mixtures of the well-characterized phases or partially hydrated materials.[13] All the metastable phases undergo an irreversible phase change to α-AlF_3 at temperatures between 450 and 650 °C.

There is some discrepancy in the literature as to which aluminum fluoride phase is formed during the fluorination procedures over γ-Al_2O_3, if a crystalline phase is formed at all.[7] Some authors report the formation of the α-phase,[3−5] while some also note the presence of the β-phase, when either alumina aerogels or γ-Al_2O_3 are used as the starting material.[14,15] The formation and catalytic activity of the fluorinated phase is therefore surprising since, although the metastable β-AlF_3 phase is immediately active as a catalyst for CFC or HCFC dismutation and halogen exchange reactions,[2] the more dense, thermodynamically stable α-AlF_3 phase is not thought to be an active catalyst:[2] α-AlF_3 is generally synthesized as a low surface area material (<80 m^2/g) but in comparative studies involving catalyst samples with similar surface areas proved to be a very poor catalyst for the dismutation reaction of HCFC-22.[2] Thus, it is not clear why fluorinated aluminas, which appear structurally to be α-AlF_3, are catalytically active with respect to the dismutation reactions of CFCs or HCFCs, whereas α-AlF_3 is not. A significant concentration of defects in the resulting fluorinated alumina is thought to be responsible for the increased catalytic activity of this material,[2] although no structural data have been presented to support this suggestion.

We have developed an in situ time-resolved X-ray powder diffraction (XRD) setup that allows controlled flow of reagent gas over the sample and accurate temperature control during the powder XRD data collection. This method has been used to follow the bulk structural changes to the alumina catalyst, as a function of time and temperature, under the conditions where the catalyst becomes active for the dismutation reaction. Solid-state NMR methods were also employed to follow the chemical modifications to the surface structure that do not necessarily produce changes to the powder XRD patterns. Specifically, we have utilized $^{19}F/^{27}Al$ cross polarization (CP) MAS NMR experiments to probe the first stages of fluorination, even in the presence of bulk γ-Al_2O_3. The combined use of NMR and diffraction to study these surfaces ensures that structural changes at both the local and long-range level are probed.

Experimental Section

Sample Preparation. Anhydrous aluminum fluoride (99+%), γ-aluminum oxide (99.997%; reported surface area: 100m^2/g), and ammonium hexafluoroaluminate (99.9%) were obtained from Alfa Aesar. HCFC-22 was used as received from Scott Specialty Gases. α-AlF_3 was prepared from the anhydrous aluminum fluoride obtained from Alfa Aesar by ramping the temperature under vacuum from 25 to 650 °C at a rate of 1 °C/min. The temperature was then held at 650 °C for an additional 24 h. β-AlF_3 was prepared from ammonium hexafluoroaluminate by heating the sample from 25 to 450 °C at a rate of 1 °C/min under a flow of dry nitrogen. The sample was then held at 450 °C for an additional 10 h. XRD was used to confirm the presence of the desired structure and the purity of the samples. EDAX elemental analyses were performed to determine the Cl:Al ratio on an ISI-SX30 scanning electron microscope, with an accelerating voltage of 15 keV. The fluorine content could not, however, be quantitatively determined with this instrument.

Dehydrated samples of γ-Al_2O_3 were prepared under vacuum by heating the sample to 300 °C at a rate of 1 °C/min, and holding at that temperature for 5 h. The samples were packed in glass tubes designed so as to allow flame sealing to form small ampules for the NMR experiments. HCFC-22 was adsorbed at room temperatures on the dehydrated sample of γ-Al_2O_3. Loading levels were established by monitoring the pressure drop with an absolute pressure gauge over a carefully calibrated vacuum line. Typically, approximately 5×10^{-6} mol of HCFC-22 were sorbed on 0.025 g of γ-Al_2O_3. The glass tubes were then flame-sealed to form ampules. During the sealing process, the sample was cooled with liquid nitrogen to prevent any reaction of the gas.

Reaction Studies. A Hewlett-Packard 6890 Series gas chromatograph (G.C.) equipped with a thermal conductivity detector and a fluorocarbon specific fused silica capillary column from J&W Scientific

(10) Le Bail, A.; Jocoboni, C.; Beblanc, M.; De Pape, R.; Duroy, H.; Fourquet, J. L. *J. Solid State Chem.* **1988**, *77*, 96−101. Christoph, F. J.; Teufer, G. U.S. Patent 3,178,483, 1965.

(11) Le Bail, A.; Fourquet, J. L.; Bentrup, U. *J. Solid State Chem.* **1992**, *100*, 151−159.

(12) Herron, N.; Thorn, D. L.; Harlow, R. L.; Jones, G. A.; Parise, J. B.; Fernandez-Baca, J. A.; Vogt, T. *Chem. Mater.* **1995**, *7*, 75−83.

(13) Alonso, C.; Morato, A.; Medina, F.; Guirado, F.; Cesteros, Y.; Salagre, P.; Sueiras, J. E.; Terrado, R.; Giralt, A. *Chem. Mater.* **2000**, *12*, 1148−1155. Shinn, D. B.; Crocket, D. S.; Haendler, H. M. *Inorg. Chem.* **1966**, *5*, 1927−1933. Christoph, F. J.; Teufer, G. U.S. Patent 3,178,483, 1965.

(14) Skapin, T. *J. Mater. Chem.* **1995**, *5*, 1215−1222. Skapin, T.; Kemnitz, E. *Catal. Lett.* **1996**, *40*, 241−247.

(15) Hess, A.; Kemnitz, E.; Lippitz, A.; Unge, W. E. S.; Menz, D. H. *J. Catal.* **1994**, *148*, 270−280.

(113-4332) was used to follow the products of the reaction of HCFC-22 over both α-AlF_3 and γ-Al_2O_3. The reaction bed was constructed from 1/4 in. 316 stainless steel tubing. Approximately 0.25 g of catalyst was packed into the reactor bed and was dried in a flow of nitrogen (40 mL/min) for 1 h at 300 °C. A thermocouple (Omega) was inserted centrally in the catalyst bed, which was held in place with quartz wool. A heating element was wrapped around the reaction bed and the thermocouple was subsequently used to control and monitor the reaction temperature. Mass flow controls (Omega) were used to control reagent flow (20 mL/min of HCFC-22) over the catalyst sample.

NMR. Variable-temperature MAS NMR experiments were performed with double-tuned 5 mm and 3.2 mm Chemagnetics probes, on a CMX-360 spectrometer. ^{27}Al and ^{19}F NMR spectra were collected at operating frequencies of 93.8 and 338.7 MHz, respectively. The double-tuned 5 mm MAS NMR probe, used to acquire spectra of the samples sealed in glass ampules, has a significant fluorine background from Teflon in the coil and capacitors. Spin−echo sequences were used to reduce the fluorine background, and were compared with simple one-pulse experiments to ensure that there was no significant loss of signal intensity or change in the relative peak intensities. The 3.2 mm MAS NMR probe has a small fluorine background only noticeable in samples with dilute concentrations of fluorine. A background spectrum collected under identical conditions was, therefore, subtracted from the spectra of these samples. Both probes use zirconia rotors capable of spinning to 21 and 10 kHz in the 3.2 and 5.0 mm probes, respectively. Variable-temperature experiments were performed with a Chemagnetics variable-temperature unit.

Small ^{27}Al flip angles were used (<15°) to ensure uniform excitation of all spins. Chemical shifts are referenced to 1 M aqueous aluminum sulfate and fluorotrichloromethane as external standards at 0.0 ppm. The Hartmann−Hahn condition for $^{19}F \rightarrow {}^{27}Al$ CP experiments was determined with anhydrous aluminum fluoride and optimized for the so-called fast spinning regime.[16] Different spinning frequencies were used for the experiments performed on the 3.2 and 5 mm probes and the contact time and Hartmann−Hahn match were optimized for each MAS frequency. The typical contact time was approximately 0.15 ms for MAS frequencies between 3 and 9 kHz. Repetition times of 1 s were used.

The ^{27}Al quadrupole coupling constants (QCCs) were determined by simulation of the ^{27}Al MAS spectra, using a program written by K. H. Lim in the GAMMA environment.[17] This program, which has been described elsewhere,[18] was used to simulate the full MAS powder pattern (i.e., the central and satellite transitions) to extract both the QCC and the asymmetry parameter η. Additional interactions such as $^{27}A-{}^{19}F$ dipolar coupling were not taken into account.

Synchrotron X-ray Powder Diffraction. X-ray synchrotron powder diffraction data were collected at the X7B beamline at the National Synchrotron Light Source (NSLS), Brookhaven National Laboratory (BNL). An image plate (IP) detector mounted perpendicular to the beam path was used to collect full-circle powder patterns. An external LaB_6 standard was used to determine the tilt angle, sample-to-detector distance, wavelength, and tilting angle of the IP.

In situ diffraction experiments were performed with a specially designed "flow cell" (Figure 2), which allows for flow of reactant gas over the sample during acquisition of powder diffraction data. The sample was packed into a 0.8 mm o.d./0.6 mm i.d. sapphire capillaries. The capillary was connected to 1/16 in. Swagelok style fittings with Vespel ferrules. A 0.010 in. thermocouple (Omega) was inserted straight into the capillary adjacent to and contacting the catalyst bed. The sample was aligned such that the sample closest to the thermocouple was in the X-ray beam path. Stainless steel tubing (1/16 in.) was used to deliver reagent gas and to connect to the same G.C. described earlier. The catalyst sample was heated by using a resistive heater placed parallel to the catalyst bed. An aluminum heat shield (with windows for the X-rays) was placed covering the heater and capillary to alleviate temperature fluctuations. The temperature was monitored and controlled by using the thermocouple placed in the catalyst bed.

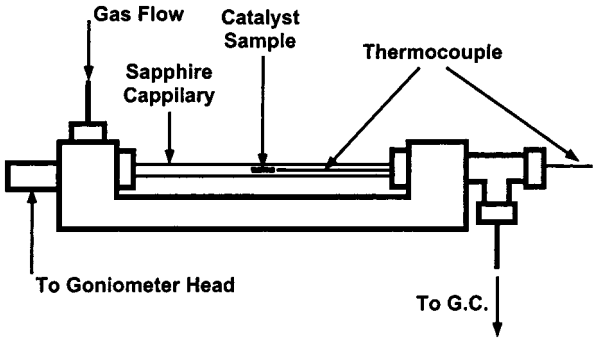

Figure 2. Diagram of the flow cell used for in situ XRD of catalysts.

Integration of the full-circle powder patterns was performed with Fit-2d,[19] excluding any reflections due to the single-crystal sapphire capillary. Rietveld refinements of the data were performed with GSAS.[20] The background was fit with a Chebyschev polynomial using 20 coefficients. The profile coefficients were fit with a pseudo-Voight function. Starting atomic coordinates were taken from those previously reported for α-AlF_3.[8] No soft constraints were used during the refinements.

Results

Reaction Studies. The product distribution for the dismutation reaction of HCFC-22 was studied over γ-Al_2O_3 and α-AlF_3 by gas chromatography. The reaction of HCFC-22 over γ-Al_2O_3 at 300 °C (Figure 3a) shows that γ-Al_2O_3 becomes active very rapidly and that the reactivity does not vary significantly over the time the reaction was monitored. The product distribution follows that expected based on the stoichiometry of the reaction. The reaction did not go totally to completion under the reaction conditions used; both residual HCFC-22 and the intermediate HCFC-21 (CCl_2FH) were observed as minor components in the product mixture. The catalyst sample, after reaction at 300 °C, shows no apparent structural changes, and only γ-Al_2O_3 is detected by laboratory XRD. A similar product distribution was observed when the reaction was performed at 400 °C (Figure 3b). Significant structural changes of the catalyst following reaction were, however, observed by XRD. The reactivity of α-AlF_3 at 300 °C was also tested, and it proved it to be a significantly less active catalyst than γ-Al_2O_3 (Figure 3c).

In situ Synchrotron X-ray Powder Diffraction. The sample of γ-Al_2O_3 was dehydrated in situ for 1 h at 300 °C and HCFC-22 flow was initiated. The temperature was then maintained at 300 °C for an hour, where after a temperature ramp from 300 to 500 °C over 3 h was performed, followed by a 1 h isothermal hold at 500 °C. Figure 4a shows a portion of the data collected during the in situ experiment from the time HCFC-22 flow was initiated to the time 425 °C was reached. The reaction results obtained from the downstream G.C. parallel those observed in the ex situ experiments (Figure 3): the γ-Al_2O_3 sample was active for the dismutation reaction of HCFC-22 from the initiation of gas flow at 300 °C all the way to 500 °C, and the reactivity remained surprisingly constant throughout the whole experiment. No obvious structural changes to γ-Al_2O_3 were seen at 300 °C, but the diffraction experiment does not rule out the possibility of low-level fluorination of the surface. During the temperature ramp, a new phase began to appear at approximately

(16) Vega, A. J. *Solid State Nucl. Magn. Reson.* **1992**, *1*, 17−32.
(17) Smith, S. A.; Levante, T. O.; Meier, B, H.; Ernst, R. R. *J. Magn. Reson.* **1994**, *106*, 75−105.
(18) Kwang Hun Lim, Ph.D. Thesis, SUNY, Stony Brook, January 2000.
(19) Hammersley, A. P. *ESRF Internal Report*, **ESRF98HA01T**, FIT2D V9.129, Reference Manual V3.1, 1998. Hammersley, A. P.; Svenson, S. O.; Hanfland, M.; Hauserman, D. *High Presssure Res.* **1996**, *14*, 235−248.
(20) Larson, A. C.; Von Dreele, R. B. *GSAS General Structure Analysis System*; Report LAUR 86-748, Los Alamos National Laboratory, New Mexico, 1995.

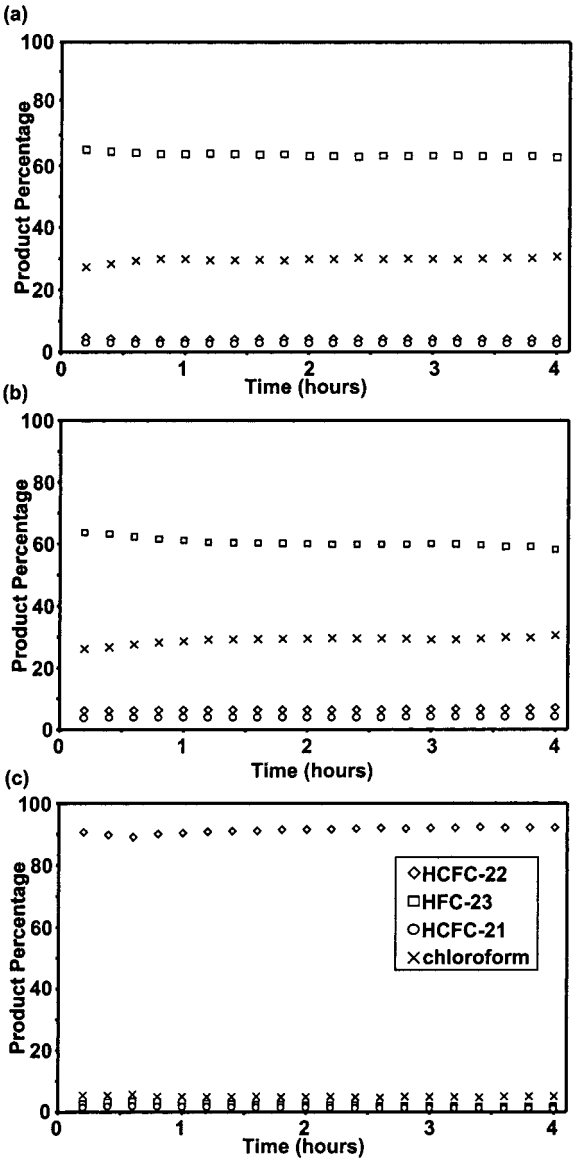

Figure 3. Product distribution for the reaction of HCFC-22 over γ-Al_2O_3 at (a) 300 and (b) 400 °C. (c) Reaction of HCFC-22 over α-AlF_3 at 300 °C.

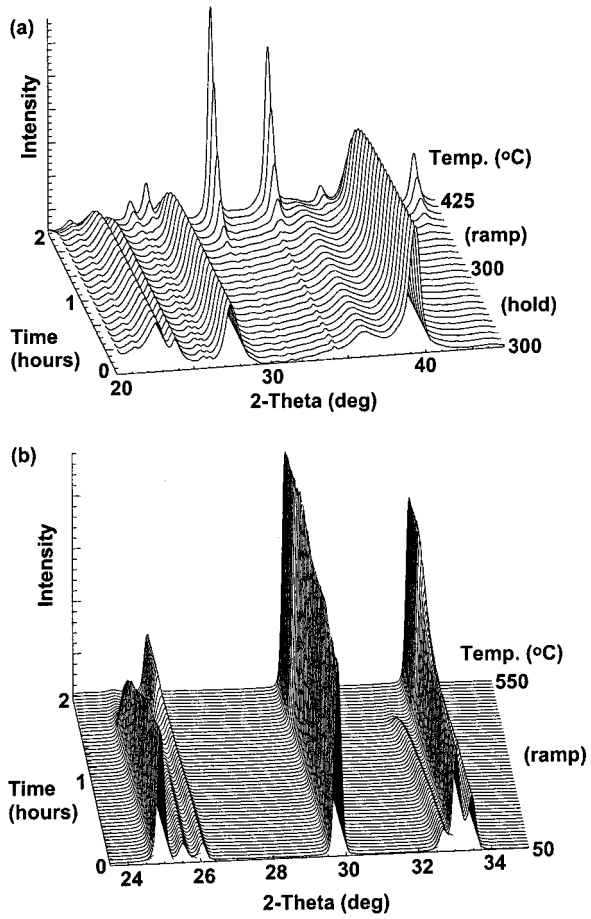

Figure 4. (a) Results of the in situ XRD experiment of γ-Al_2O_3 under HCFC-22 flow. From 0 to 1 h the temperature was kept isothermal at 300 °C. From 1 to 2 h the temperature was ramped slowly to 425 °C (λ = 0.9033 Å). (b) α-AlF_3, ramped from 50 to 550 °C in 2 h (λ = 0.9033 Å).

360 °C, as seen by the two intense reflections at 30.4 and 34.0° 2θ. The final diffraction pattern extracted from the time-resolved plot (Figure 5a) reveals that the γ-Al_2O_3 has been completely transformed into a different structural phase by 500 °C.

Neither the final diffraction pattern recorded at the end of the temperature ramp (500 °C, Figure 5a) nor that of the final material following cooling to ambient temperature (50 °C, Figure 5b) could be easily indexed based on the known phases of AlF_3. Results from ex situ NMR experiments (see below) suggested that the material was structurally related to α-AlF_3. In addition, close examination of the powder patterns revealed a similarity between many of the reflections of the catalyst and those of α-AlF_3. Thus, to aid in the understanding of the structural changes of the catalyst during activation and reaction, an in situ temperature ramp of α-AlF_3 was performed, Figure 4b. To allow direct comparisons to be made, the same flow cell apparatus was used for the temperature ramp of α-AlF_3, although no gas flow was used. A noticeable phase transition to a less distorted phase was observed at 460 °C (1.6 h), close to the reported phase-transition temperature,[8,9] as witnessed by the sudden decrease in intensity of, for example, the 113 reflection at 24.6° 2θ. Surprisingly, however, a complete rhombohedral to cubic phase transition was not observed even up to 550 °C: for example, a weak reflection (113) near 25° 2θ persists at 500 °C (Figure 5c), consistent with a small rhombohedral distortion.

Given the noticeable similarity between the high-temperature structure of α-AlF_3 and that of the catalyst, refinement of the catalyst structure using the structural model of α-AlF_3 was performed. Details of the refinements of the catalyst (at 50 and 500 °C) are compared with those for α-AlF_3 (at 50 and 500 °C) in Table 1, and the final refinements are shown in Figure 5. The structure of α-AlF_3 was refined as a function of temperature using powder patterns periodically extracted from the time-resolved plots to obtain the Al−F−Al bond angles shown in Figure 6. A small portion of the diffraction pattern (from 31.5 to 32.5° 2θ) was excluded from the refinement of the catalyst at 500 °C (Figure 5a), due to the presence of a reflection from the sapphire capillary which was not, upon closer examination, excluded during the integration of the full circle powder patterns. The plots of the displacement ellipsoids for both structures at 50 and 500 °C are shown in Figure 7.

NMR. ^{19}F and ^{27}Al MAS NMR spectra were recorded for γ-Al_2O_3, and the model compounds α-AlF_3 and β-AlF_3 (Figure 8). The ^{27}Al NMR spectra of γ-Al_2O_3 reveals two resonances, one at 9 ppm attributable the octahedral aluminum environment and the other at 67 ppm due to aluminum in the tetrahedral environment (Figure 8a). The ^{27}Al NMR spectra of α-AlF_3 and β-AlF_3 show resonances at −16 and −15 ppm, respectively,

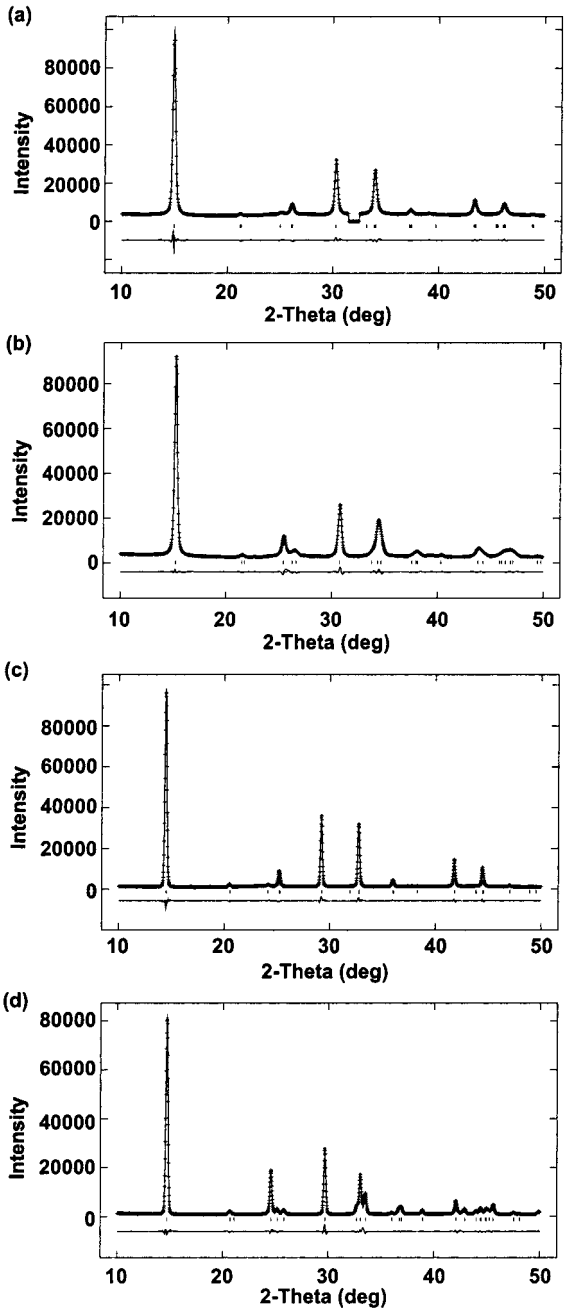

Figure 5. Refinements of "used" catalyst at (a) 500 and (b) 50 °C ($\lambda = 0$. 0.9391 Å). Refinements of the α-AlF_3 at (c) 500 and (d) 50 °C ($\lambda = 0.9033$ Å).

which can be assigned to Al in an octahedral AlF_6 environment (Figure 8b,c). The ^{19}F MAS NMR of α- (Figure 8d) and β-AlF_3 (Figure 8e) are essentially identical. Thus α- and β-AlF_3 cannot be distinguished based on their ^{27}Al NMR and ^{19}F chemical shifts. The widths of the ^{27}Al sideband manifolds of α-AlF_3 and β-AlF_3 are very different, however, suggesting a method for distinguishing between these two structures by NMR. These sidebands arise from the ^{27}Al satellite transitions and, thus, the broader β-AlF_3 spectrum indicates a larger QCC for this phase, and thus a more distorted aluminum environment. Simulations of these spectra yielded a value for the QCC of α-AlF_3 of 0.23 ± 0.02 MHz; the value of η was fixed to be 0 in these simulations due to the site symmetry at the Al site ($\bar{3}$). Slower spinning spectra are required to determine, with any level of accuracy, whether there are any deviations from this value due to any local distortions. A QCC of 0.8 ± 0.1 MHz and a value for η of 0.8 ± 0.1 were determined for the lower symmetry sites in β-AlF_3. These results differ significantly from the values previously reported in the literature of 2.8 ($\eta = 0$) and 3.4 MHz ($\eta = 0$) for α- and β-AlF_3, respectively.[21]

Table 1. Crystallographic Information

	catalyst (25 °C)	catalyst (500 °C)	α-AlF_3 (25 °C)	α-AlF_3 (500 °C)
crystal system	rhombo-hedral	rhombo-hedral	rhombo-hedral	rhombo-hedral
space group	$R\bar{3}c$	$R\bar{3}c$	$R\bar{3}c$	$R\bar{3}c$
Z	6	6	6	6
cell parameters				
a, Å	4.9772(7)	5.0543(3)	4.9381(5)	5.0549(2)
c, Å	12.388(2)	12.441(1)	12.424(1)	12.3997(8)
density, g·cm^{-3}	3.148	3.040	3.189	3.049
wavelength, Å	0.9391	0.9391	0.9033	0.9033
2θ range, deg	5−52	5−52	5−52	5−52
χ^2	7.5	5.8	8.5	4.2
R	0.019	0.016	0.029	0.018
R_p	0.027	0.025	0.040	0.027
R_{wp}	0.039	0.033	0.060	0.040

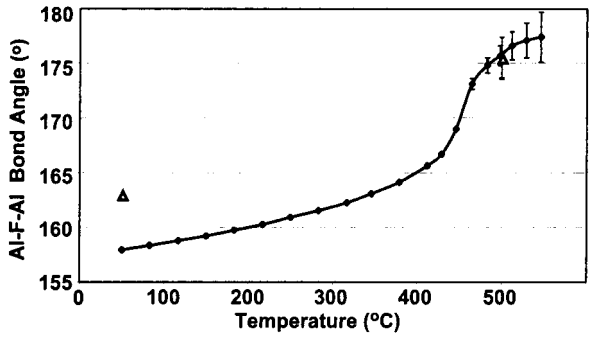

Figure 6. Al−F−Al bond angle as a function of temperature for α-AlF_3 (line) and the "used" catalyst (triangles).

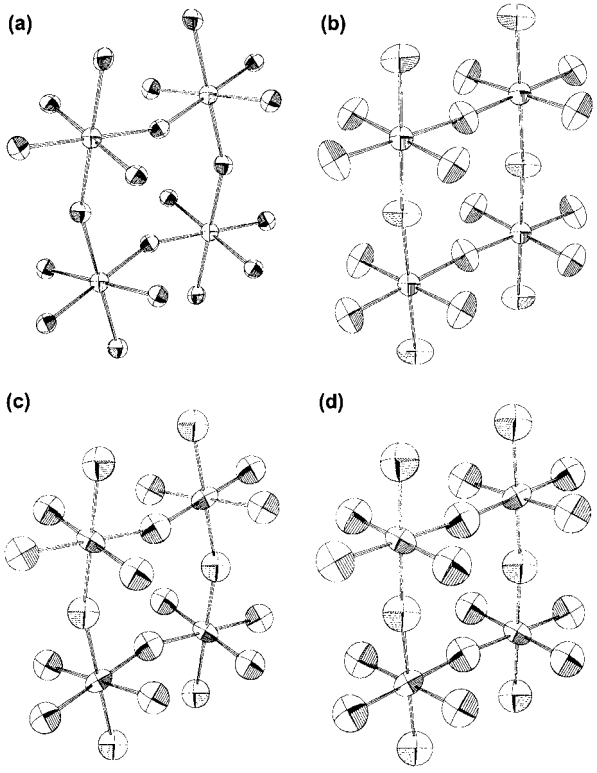

Figure 7. Displacement ellipsoids shown at 50% probability. α-AlF_3 at (a) 25 and (b) 500 °C. Used catalyst at (c) 25 and (d) 500 °C.

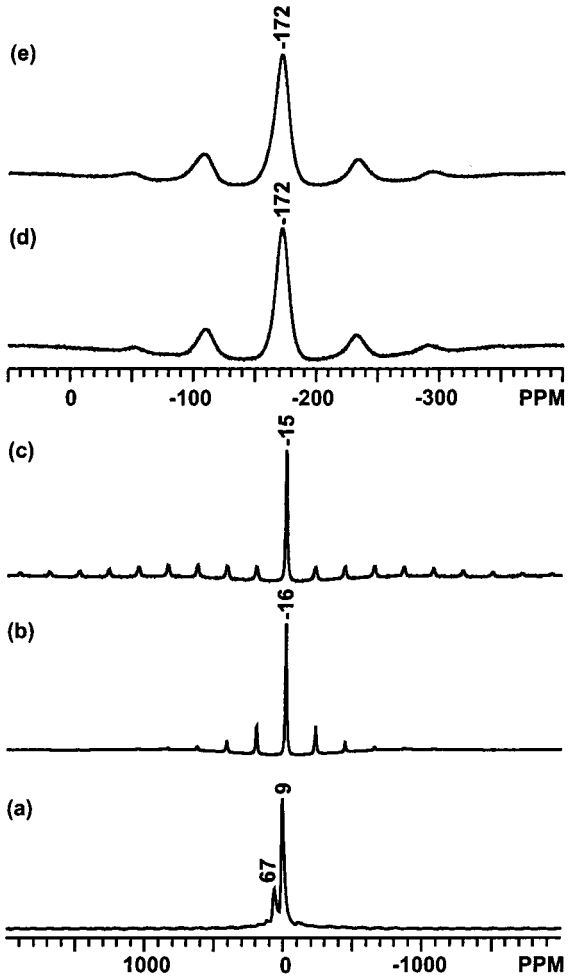

Figure 8. ^{27}Al MAS NMR of (a) γ-Al_2O_3, (b) α-AlF_3, and (c) β-AlF_3. ^{19}F MAS NMR of (d) α-AlF_3 and (d) β-AlF_3. Spectrum a was collected at a spinning frequency, ν_r, of 10 kHz, while spectra b−e were collected at 20 kHz.

Catalyst samples were prepared, ex situ, by HCFC-22 flow over γ-Al_2O_3 for 4 h at isothermal conditions at either 300 or 400 °C. Figure 9 shows the ^{19}F and ^{27}Al spectra of the catalyst prepared at 300 °C. Only γ-Al_2O_3 is visible in the ^{27}Al spectrum (Figure 9a), and there is no indication of any fluorination. A $^{19}F/^{27}Al$ CP NMR experiment (Figure 9b) was therefore performed to select the aluminum environments near fluorine. As can be seen from the resulting spectrum, a resonance consistent with Al−F octahedral environments is observed. Two resonances are observed in the ^{19}F spectrum (Figure 9c): the resonance at −168 ppm is consistent with an octahedral AlF_6 environment, while the other resonance at −146 ppm is assigned to either an AlF_xO_{6-x} ($1 < x < 5$) environment or a terminal fluorine atom at the surface. These results are consistent with those from the diffraction experiments where no structural changes were observed at 300 °C.

The catalyst prepared ex situ at 400 °C clearly shows the presence of an aluminum fluoride phase in the ^{27}Al spectrum (Figure 10a), with a QCC that is similar to that of α-AlF_3, as seen by the similar spinning-sideband patterns. Careful comparison of the intensities of the satellite transitions in the two spectra reveal a distribution of QCCs for the catalyst, some sites being present in the catalyst with slightly larger QCCs. A trace amount of γ-Al_2O_3 is still present resulting in the weaker

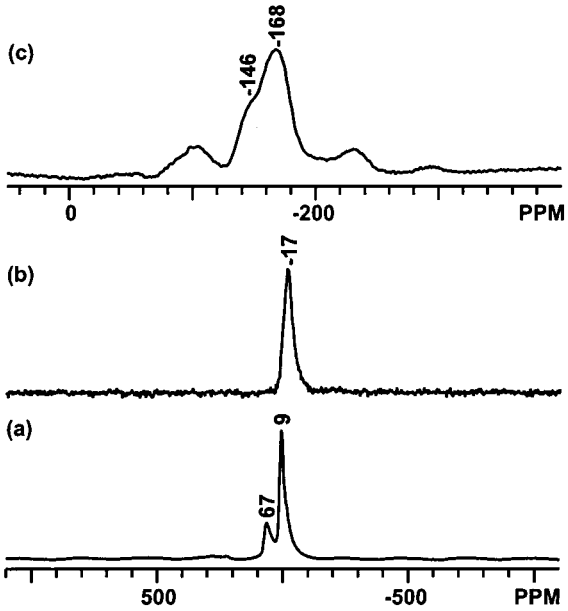

Figure 9. Catalyst prepared ex situ at 300 °C: (a) ^{27}Al MAS NMR ($\nu_r = 10$ kHz); (b) $^{19}F/^{27}Al$ CP NMR ($\nu_r = 10$ kHz); and (c) ^{19}F MAS NMR ($\nu_r = 20$ kHz).

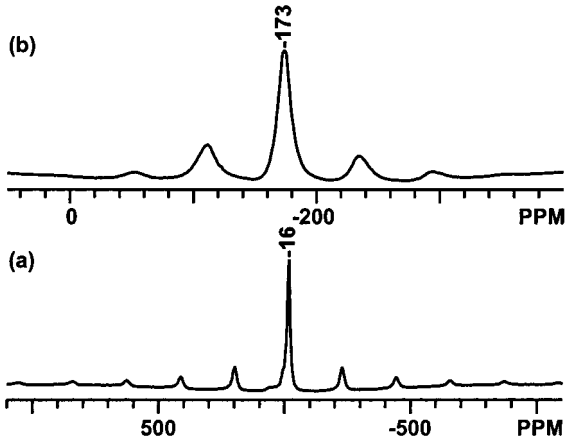

Figure 10. Catalyst prepared ex situ at 400 °C: (a) ^{27}Al MAS NMR ($\nu_r = 20$ kHz) and (b) ^{19}F MAS NMR ($\nu_r = 20$ kHz).

resonances at higher frequencies than the AlF_6 resonance at −16 ppm. The ^{19}F spectra show a single resonance at −173 ppm, which is again consistent with AlF_3 and similar to the resonance of either α- or β-AlF_3. Again these results are consistent with the diffraction experiments where at temperatures between 300 and 400 °C fluorination of the bulk of γ-Al_2O_3 is observed in conjunction with the formation of a new phase.

To probe the initial stages of the fluorination in more detail, reaction studies were performed by performing NMR experiments on sealed samples of HCFC-22 over dehydrated γ-Al_2O_3. Two sets of resonances are observed in the initial ^{19}F spectrum prior to any heat treatment (Figure 11a). A sharp doublet at −76 ppm is attributed to free/gaseous HCFC-22, the doublet arising from $^1H-^{19}F$ *J*-coupling. The broad resonance at −74 ppm is assigned to physisorbed HCFC-22. Variable-temperature experiments of the γ-Al_2O_3 samples were performed to verify the assignments, the intensities of the resonances of the physisorbed molecules increasing (at the expense of that of those from the free gases) as the temperature is lowered. Spectra of gaseous HCFC-22 and HFC-23, sealed in gas ampules, further confirmed the assignments. The sealed γ-Al_2O_3/HCFC-22 sample was heated at 300 °C for 15 min, quenched immediately

(21) Dirken, P. J.; Jansen, J. B. H.; Schuiling, R. D. *Am. Miner.* **1992**, *77*, 718−724.

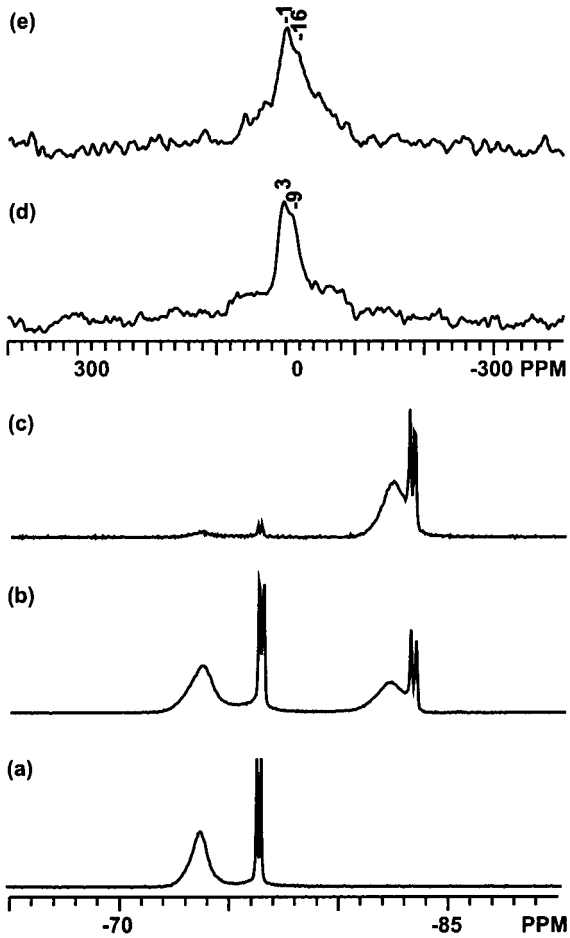

Figure 11. (a) ^{19}F MAS NMR of HCFC-22 adsorbed on γ-Al_2O_3 and sealed in a glass ampule ($\nu_r = 3$ kHz). (b) ^{19}F MAS NMR of the same sample heated at 300 °C for 15 min ($\nu_r = 6$ kHz). (c) ^{19}F MAS NMR of the same sample heated at 300 °C for a total of 1 h ($\nu_r = 6$ kHz). (d) ^{19}F/^{27}Al CP NMR of the sample heated for 15 min ($\nu_r = 6$ kHz). (d) ^{19}F/^{27}Al CP NMR of the sample heated for 1 h ($\nu_r = 6$ kHz). All the ^{19}F MAS NMR spectra were collected with a rotor synchronized spin−echo sequence with a spin-evolution time (330 μs) selected to minimize the background signal.

to room temperature, and the ^{19}F spectrum acquired (Figure 11b). In addition to the originally observed resonances for HCFC-22, two additional sets of resonances are observed at −84 (a doublet) and −83 ppm (broad resonance). The doublet is assigned to free HFC-23, and the broad resonance to physisorbed HFC-23. The ^{19}F resonance due to bulk AlF_3 (−173 ppm) appears at a similar chemical shift as the broad, intense background of the probe thus it was not possible, using this probe, to determine whether any AlF_3 is formed, by ^{19}F MAS NMR. Since no fluorinated species were detected in the ^{27}Al one-pulse spectrum, a ^{19}F/^{27}Al CP NMR experiment was performed. A very weak signal was obtained (Figure 11d) in the region from 3 to −9 ppm. This chemical shift is intermediate between those of AlO_6 and AlF_6 local environments. The intensity of the cross-polarization signal in all the experiments was found to be extremely sensitive to the frequency of the ^{19}F irradiation. In the spectrum shown in Figure 11d (and in Figure 9b), the ^{19}F carrier frequency was placed on resonance at −168 ppm, which resulted in the maximum signal intensity, indicating that the ^{27}Al signal arises from fluorine species with ^{19}F chemical shifts in this range. Experiments were also performed where the ^{19}F irradiation frequency was systematically varied to ensure that ^{27}Al signals from other fluorine species were not ignored, but no additional ^{27}Al resonances were detected.

The sample was then heated for another 45 min at 300 °C and the ^{19}F spectrum shows a proportionately larger amount of HFC-23 and only a trace amount of HCFC-22. No resonances attributable to dichlorofluoromethane (CCl_2FH or HCFC-21) were seen, the reaction proceeding to completion in the static reaction vessel. The ^{19}F/^{27}Al CP NMR experiment was then performed and a broad resonance stretching from −1 to −16 ppm was observed. The shift of the ^{27}Al resonance to lower frequency following the longer heat treatment is consistent with the increased level of fluorination of the Al−F local environments. Since HCFC-22 is used as the fluorinating agent it is likely that there may be chlorine on the surface in addition to fluorine. The ^{27}Al chemical shift for solid $AlCl_3$, which contains octahedral $AlCl_6$ environments, is approximately 0 ppm.[22] Thus, substitution of the AlO_6 local environment by a F or Cl atom is predicted to result in a shift of the ^{27}Al resonance by −4 or −1.5 ppm, respectively, to a first approximation. Therefore the resonances can be assigned to local environments such as $AlO_{6-x-y}F_xCl_y$, where $x > 0$ and $x + y$ is most likely between 2 and 4 for short reaction times and 4 and 6 for longer reaction times. The value of x increases with increased reaction time, resulting in a shift toward frequencies that approach those of the bulk (−16 ppm).

Discussion

A comparison of the ^{27}Al QCCs of the model aluminum fluorides with that determined for the fluorinated catalyst clearly indicates that the catalyst phase is closely related to α-AlF_3. This is further confirmed by similarity of the time/temperature resolved XRD powder pattern of α-AlF_3 and the fluorinated catalyst. The XRD reflections in the powder pattern of the fluorinated catalyst are considerably broader than those of α-AlF_3, suggesting considerable disorder and/or small particle sizes. The high-temperature structure of α-AlF_3 shows classical displacement ellipsoids, the fluorine displacement ellipsoids being larger in the direction normal to the Al−F bond direction. This is consistent with motion involving rocking of the AlF_6 octahedra. Motion of this type has been observed previously at high temperatures for the double perovskite cryolite.[23] In contrast, the thermal displacement parameters obtained from the refinements of the catalyst are quite large, both at 500 and 25 °C (Figure 7 and Table 2). The displacement parameters are essentially isotropic and do not significantly increase in magnitude from room temperature to 500 °C, indicating that significant structural disorder is present, as opposed to disorder due to motion of, for example, the AlF_6 octahedra.

The most convenient way to characterize the difference between the catalyst and the α-AlF_3 structure is by comparison of the Al−F−Al bond angle. At 500 °C, the Al−F−Al bond angle of the catalyst is 174.5° while at 50 °C the angle is 163.0°. In comparison, the Al−F−Al bond angle of α-AlF_3 at 500 °C is 175.8° while at 50 °C it has dropped to 157.9°. Therefore, the catalyst structure seems less flexible, in that the Al−F−Al bond angle does not vary to the same extent as the Al−F−Al bond angle in α-AlF_3, over the same temperature range (Figure 6). This suggests that there is disorder or defects present that stabilize the higher temperature, less distorted structure. Since α-AlF_3 possesses only an extremely small fraction of the activity for HCFC-22 dismutation, as compared with that of fluorinated

(22) Kaikkonen, A.; Ylinen, E. E.; Punkkinen, M. *Solid State Nucl. Magn. Reson.* **1998**, *10*, 129−135.
(23) Yang, H.; Ghose, S.; Hatch, D. M. *Phys. Chem. Miner.* **1993**, *19*, 528−544.

Table 2. Positional and Thermal Displacement Parameters

(a) Positional Parameters (Al; 0, 0, 0) (F; x, 0, 0.25)

sample	fluorine × position	F−Al−F angle (deg)	Al−F distance (Å)
catalyst (25 °C)	0.4470(5)	163.04(26)	1.78870(27)
catalyst (500 °C)	0.4862(6)	175.5(19)	1.79123(15)
α-AlF_3 (25 °C)	0.4309(2)	157.93(15)	1.79500(22)
α-AlF_3 (500 °C)	0.4871(3)	175.8(10)	1.78923(8)

(b) Anisotropic Thermal Parameters

sample	atom	U_{11} or U_{iso}	U_{22}	U_{33}	U_{12}	U_{13}	U_{23}
catalyst (25 °C)	Al	0.030(1)	0.030(1)	0.014(1)	0.0051(5)	0	0
	F	0.053(1)	0.046(2)	0.029(2)	0.023(1)	−0.0089(6)	−0.018(1)
catalyst (500 °C)	Al	0.038(2)	0.038(2)	0.023(3)	0.0089(9)	0	0
	F	0.074(3)	0.054(4)	0.043(3)	0.027(2)	−0.012(1)	−0.024(3)
α-AlF_3 (25 °C)	Al	0.021(1)	0.021(1)	0.019(1)	0.0104(3)	0	0
	F	0.023(1)	0.021(1)	0.022(1)	0.0106(4)	−0.0105(3)	−0.0080(7)
α-AlF_3 (500 °C)	Al	0.0267(3)					
	F	0.056(2)	0.041(3)	0.026(2)	0.020(1)	−0.026(1)	−0.022(2)

alumina, this suggests that the defects that occur during fluorination of alumina, and that are present on the surface of the newly formed catalyst, are responsible for the dramatic increase in catalytic activity.

Many plausible schemes exist for the incorporation of disorder into the bulk fluorinated catalyst phase. Chlorine from the HCFC-22 molecule could be incorporated into the structure. Preliminary EDAX elemental analysis results of the sample prepared ex situ for NMR studies at 400 °C definitively show that small amounts of chlorine are present. If the chlorine is assumed to be distributed evenly throughout the material then a composition of $AlF_{2.94}Cl_{0.06}$ is obtained. It is unclear at this point whether the chlorine resides at the surface or in the bulk of the material, and further investigations are underway to determine the location of the chlorine within the structure. Residual oxygen atoms may remain in the structure, in both the protonated and nonprotonated forms. Incorporated oxygen atoms with no associated protons would lead to associated anion vacancies or cation interstitials to achieve overall charge balance of the structure. The degree of disorder present appears to be linked with both the sample preparation method (temperature and starting material) and fluorinating agent. For example, our preliminary results for fluorination with both HCFC-22 and HFC-23 at higher temperatures (500 °C) show that an aluminum fluoride that contains fewer defects and that more closely resembles α-AlF_3 is formed. Furthermore, prolonged calcination at high temperatures of the material fluorinated at lower temperature results in some annealing of the material and an increase in crystallinity. This suggests that the defects arise from the low fluorination temperature and are not necessarily a consequence of the incorporation of high concentrations of substitutional defects. This is in agreement with the NMR results, where no clear evidence was seen in the catalyst prepared at 400 °C, for the broad distribution of ^{27}Al chemical shifts that would result from high concentrations of substitutional AlO_xF_{6-x} or $AlCl_yF_{6-y}$ defects in the lattice. Furthermore, the $^{19}F/^{27}Al$ CP results for the catalyst fluorinated at 300 °C for 15, 45, and 4 h show that even at these low fluorination levels and low temperatures, the surface reaction proceeds via a distribution of substituted aluminum local environments ($AlO_xCl_yF_{6-x-y}$) (Figure 11) to form, after 4 h of fluorination, AlF_6 species and no other aluminum fluoride local environments (Figure 9b).

Clearly, fluorination of bulk alumina does not become energetically favorable until temperatures of 360 °C and above. Although fluorination of the first few surface layers does occur at 300 °C, as seen by $^{19}F/^{27}Al$ CP NMR, no evidence for any growth of a crystalline phase is, however, seen at this temperature. Fluorination of the surface can proceed via the loss of oxygen in the form of CO_2, as seen in the previous IR study of the decomposition of CFCs.[7] In the case of a HCFC, the following equation can be written for the fluorination of the bulk phase:

$$2HCF_2Cl + Al_2O_3 \rightarrow H_2O + 2AlF_2Cl + CO$$

CO can disproportionate to form C and CO_2, accounting for the coking seen on the catalyst prepared ex situ at 400 °C. Unfortunately, we were unable to probe CO_2 formation with our current G.C. setup due to the proximity of the CO_2 and N_2 peaks eluted out of our GC column; CO was, however, detected during the ex situ experiments at 400 °C. The chlorine may be removed from the surface via the reaction with surface hydroxyls, generally present on γ-Al_2O_3, and the formation of HCl. Corrosion of parts of our reactor is often observed following these reactions, which we believe may be the result of this HCl evolution. In addition, the chlorine species can react with HCFC-22 to generate HCFC-21 and eventually chloroform.

The importance of chlorine on the modification of Lewis acidity, and thus reactivity of aluminum trifluoride or alumina, should not be overlooked.[24] For example, $AlCl_3$ fluorinated with CFCs or HCFCs produces an anhydrous material referred to as aluminum chlorofluoride (ACF), with the approximate formula AlF_xCl_y, where $2.8 < x < 2.9$ and $0.1 < y < 0.2$.[24] This material has interesting properties in that it is essentially amorphous, has comparable Lewis acidity to SbF_5, and has been reported to be a highly active catalyst with regards to the disproportionation of CFCs or HCFCs. ACF cannot be fully fluorinated otherwise it loses its catalytic activity. An analogy can obviously be drawn between ACF and alumina fluorinated with CFCs or HCFCs. Studies of the early stages of the fluorination reaction over γ-Al_2O_3 are currently underway to determine the role of chlorine in these reactions.

Conclusions

The work reported in this paper demonstrates that in situ synchrotron XRD methods may be used to determine the nature of the phases present during a catalytic reaction. The disap-

(24) Krespen, C. G.; Petrov, V. A. *Chem. Rev.* **1996**, *96*, 9−3301. Krespen, C. G. U.S. Patent 5,162,594.

pearance of the original catalyst and the growth of any new phases may be directly monitored, under operating conditions. Use of a G.C. system, downstream of the catalyst bed, ensures that structural changes can be directly correlated with catalytic behavior. By using MAS NMR methods, we were able to monitor the first stages of the evolution of the catalyst, before any new crystalline phases are observed.

The fluorination of alumina results in a material that is nominally AlF_3 but has drastically different catalytic activity from α-AlF_3. Both in situ powder diffraction and solid-state NMR were employed to investigate the cause of this enhanced catalytic activity, and determine the structure of this material. Rietveld analyses of the time-resolved powder patterns showed that the fluorinated phase that grows on γ-Al_2O_3 resembles α-AlF_3 but contains significant static disorder, as seen by the large thermal ellipsoids. This disorder appears to affect the flexibility of the catalyst phase, so that smaller changes in the extent of the rhombohedral distortion (as monitored by the Al−F−Al bond angle) are seen as a function of temperature, in comparison to the changes seen for α-AlF_3 in the same temperature regime. Refinements of the structure of α-AlF_3, as a function of temperature, show that the high-temperature version of this phase still contains a small rhombohedral distortion.

Solid-state NMR proved to be a valuable tool for studying low levels of fluorination on the surface of the alumina. This chemical modification of the surface was not apparent in the XRD. Furthermore, use of $^{19}F/^{27}Al$ CP NMR methods allowed these small levels of fluorination to be detected, even in the presence of high concentrations of the bulk phase (γ-Al_2O_3). An NMR approach was also presented to determine which aluminum fluoride phase grows on the surface of the catalyst, based on the differences of the QCCs of the α- and β-AlF_3 phases. This information helped in the interpretation of the XRD results.

Finally, since fluorinated alumina is a widely used catalyst and catalyst support material, extensions of this approach to study a variety of catalytic reactions may be readily envisioned.

Acknowledgment. Thomas Krawietz is thanked for his help with some of the initial stages of this project. Financial support from the Basic Energy Sciences program of the Department of Energy is gratefully acknowledged (DEFG0296ER14681); C.P.G. thanks DuPont for support via a Young Professor Award. The research at BNL was supported under contract DE-AC02-98CH10886 with the D.O.E. by its Division of Chemical Sciences, Office of Basic Energy Research.

JA0032374